Research Square

Preprints are preliminary reports that have not undergone peer review.
They should not be considered conclusive, used to inform clinical practice,
or referenced by the media as validated information.

Integrated Computational and Experimental Study Reveals Isorhoifolin as a Potential Therapeutic Agent Against Hepato-cellular Carcinoma Through Putative EGFR and CYP1B1 Interactions

Xiang Ji
Tongchuan Mining Bureau Central Hospital
Feng-mei Li
Tongchuan Mining Bureau Central Hospital
Chen Chen
Tongchuan Mining Bureau Central Hospital
Hong-zhong Yang
Tongchuan Mining Bureau Central Hospital
Li-min Shao
Tongchuan Mining Bureau Central Hospital
Ni Li
Tongchuan Mining Bureau Central Hospital
Ying Zhang
2448135540stu.xjtu.edu.cn

Tongchuan Mining Bureau Central Hospital

Article

Keywords: Chaihu Shugan San, Isorhoifolin, hepatocellular carcinoma, network pharmacology, molecular docking, molecular dynamics simulation

Posted Date: August 13th, 2026

DOI: https://doi.org/10.21203/rs.3.rs-10518068/v1

License: This work is licensed under a Creative Commons Attribution 4.0 International License.
Read Full License

Additional Declarations: No competing interests reported.

Integrated Computational and Experimental Study Reveals *Isorhoifolin* as a Potential Therapeutic Agent Against Hepato-cellular Carcinoma Through Putative EGFR and CYP1B1 Interactions

Xiang Ji[1], Feng-mei Li[1], Chen Chen[1], Hong-zhong Yang[1], Li-min Shao[1], Ni Li1, Ying Zhang[1, 2, *]

[1] Department of pharmacy, Tongchuan Mining Bureau Central Hospital, Tongchuan 727000, China;

[2] School of Pharmacy, Xi'an Jiaotong University, 76 Yanta West Road, Xi'an, 710061, Shaanxi, China;

* Correspondence: 244813554@stu.xjtu.edu.cn;

Abstract

Chaihu Shugan San (CSS), a well-established traditional Chinese medicine formula, has demonstrated anticancer effects on hepatocellular carcinoma (HCC). However, the main active components and the mechanism of action of CSS are not clear. We aimed to de-termine the main anti-HCC ingredient of CSS and clarify its therapeutic mechanisms us-ing computational and experimental approaches.

A network pharmacology approach was used to find therapeutic targets of CSS for HCC and perform GO and KEGG analyses of its related pathways and functions. CSS-derived compounds and HCC-related targets were evaluated via molecular docking. The optimal compound-target interactions were characterized via 500 ns molecular dynamics (MD) simulations, free energy landscape (FEL) analysis, and MM/PBSA calculations. Finally, we evaluated the *In vitro* anti-HCC efficacy of the lead compound in HepG2 and Huh7 cells through MTT assay, cell proliferation and Annexin V-FITC/PI assays. Network pharmacology predicted many targets associated with oxidative stress, chemical carcin-ogenesis, nitrogen metabolism and receptor signaling pathways for CSS in the regulation of HCC.

Molecular docking screened two top compounds namely *Isorhoifolin* and 3,5,6,7,8,3,4-heptamethylflavone. In MD simulation analysis, the docked complexes formed by *Isorhoifolin* and its targets were relatively stable compared with corresponding controls. According to MM/PBSA, *Isorhoifolin* had relatively strong binding ability with EGFR (-274.20 kJ/mol) compared to Erlotinib (-234.21 kJ/mol) and with CYP1B1 (-383.03 kJ/mol) compared to 2-Phenylquinazoline-4-amine (-142.81 kJ/mol). *In vitro* experiments showed that *Isorhoifolin* inhibit HCC viability (IC_{50} value of 20.48 μM in HepG2 cells and 26.93 μM in Huh7 cells), suppressed HCC cell proliferation in dose-dependent manner and induced apoptosis of HCC cells.

The study identified *Isorhoifolin* as a key anti-HCC bioactive ingredient in CSS and demonstrated potent anti-HCC activity and exhibited predicted interactions with EGFR and CYP1B1 in computational analyses, based on integrating multi-scale approaches.

Keywords: *Chaihu Shugan San*; *Isorhoifolin*; hepatocellular carcinoma; network pharmacology; molecular docking; molecular dynamics simulation.

1. Introduction

Hepatocellular carcinoma (HCC), the most common primary tumor of the liver, is one of the top causes of cancer-related death globally (Li et al., 2026). Although significant advances in surgical resection, liver transplantation, loco-regional therapy, and targeted therapy have been made, the prognosis of advanced HCC is still poor owing to heterogeneity, frequent recurrence, metastasis, and the rapid development of drug resistance (Chidambaranathan-Reghupaty et al., 2021). Many molecular targeted agents, including sorafenib, Lenvatinib, and erlotinib-based targeted therapy, have improved clinical outcomes of specific HCC patients but often cause side effects and are easily overcome by drug resistance (Ladd et al., 2024). Thus, developing new targeted agents with multiple targets would be a viable approach.

As an abundant resource of compounds with multiple biological functions for cancer therapy due to multi-target and multi-component characteristics, traditional Chinese medicine (TCM) has gradually received increased attention (Li et al., 2025). A classical prescription *Chaihu Shugan San* (CSS), first found in the book *Jingyue Quanshu*, was traditionally used for regulation of the stagnant liver to alleviate pain and is composed of seven medicinal plants, including *Bupleuri Radix, Paeoniae Radix Alba, Citri Reticulatae Pericarpium, Aurantii Fructus, Cyperi Rhizoma, Glycyrrhizae Radix et Rhizoma* and *Chuanxiong Rhizoma* (Zhang et al., 2024). Previous studies showed that CSS has been reported with the pharmacological properties of anti-inflammation, antioxidant, anti-fibrotic and anti-cancer effect (Xie et al., 2022). However, it is still obscure what kind of molecular mechanism is responsible for anti-HCC effect of CSS due to complex component. The networks pharmacology method, which integrates high-throughput "omics" data and the "gene-network-disease" modeling, allows system-level analysis of complex herb-compound-target-disease relationships and represents a powerful approach for discovery of new drug and mechanism of drugs (Zhai et al., 2025). Combining with molecular docking and Molecular Dynamics (MD) simulation, this method is widely used for predicting the active compounds and mechanisms of TCM (Ye et al., 2026). However, the computation approach cannot be fully proven to guide experimental drug design, so validation should be done at the experimental level. In this study, we collected the active ingredients of CSS from literature.

SwissTargetPrediction tool was used to screen the potential targets of the active ingredients and screened the target related to HCC through disease-gene relationship analysis. Further analysis using gene ontology enrichment analysis, protein–protein interaction (PPI) network and expression analysis was performed to predict key therapeutic targets of CSS against HCC. Then, we used the Molecular Docking, MD simulations, FEL analysis and Molecular Mechanics/Poisson–Boltzmann Surface Area (MM/PBSA) calculation to study ligand–target interaction of the top active ingredient. Finally, the predicted active compound was validated in HepG2 and Huh7 cells.

We have identified that *Isorhoifolin* is a promising bioactive constituent of CSS acting against HCC. This study provides new insight into the potential molecular targets and mechanism of action of *Isorhoifolin* on HCC.

2. Results

2.1 Identification of potential therapeutic targets of CSS against hepatocellular carcinoma

121 chemical compounds were obtained from previously published phytochemical analyses of CSS. The canonical SMILES strings were obtained from PubChem and entered into the SwissTargetPrediction server to identify possible targets. Duplicated targets were removed to obtain 1,163 potential protein targets. 48 high confidence target proteins were selected according to their predicted values of (prediction probability) > 0.30, to guaran-tee reliable predicted values. 19063 coding protein genes associated with liver cancer were acquired from the GeneCards database to screen potential therapeutic targets for HCC. A Venn diagram constructed with an R programming language showed that the 48 predicted high confidence targets of CSS are all present within the gene set of liver cancer-related genes. The 48 high confidence target protein compounds of CSS have the high relevance with liver cancer (Figure 1). We performed the network pharmacology analysis based on the above information.

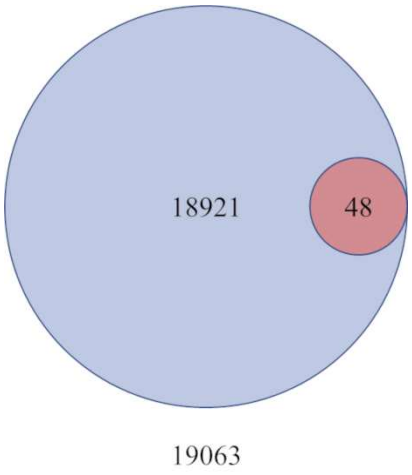


Figure 1. Identification of overlapping targets between CSS-derived compounds (red circle) and HCC-related genes (blue circle). A total of 48 overlapping genes were identified.

2.2 Construction of the compound–target–HCC interaction network

In order to clearly present the relationships of herbal medicines, active compounds, potential targets and HCC, a compound-target-disease interaction network was established and displayed using Cytoscape (Figure 2). After a collection of 121 compounds in total, only 29 compounds interacted with the 48 high-confidence targets; thus, it could be assumed that these components are chiefly responsible for the predicted bio-pharmacological activity of CSS. These compounds are from each of the seven individual ingredients, demonstrating the multi-component attribute of CSS. Network topology revealed that many compounds displayed much larger degree values than the others, which suggested that the given compound could act with more than one target protein, and some target protein was also targeted by a multiplicity of compounds. This reflected the "multi-component - multi-target" principle that is well characteristic of traditional Chinese medicine. In sum, compound-target network illustrated that CSS against HCC is attributed to the synergy among

various phytochemicals via molecular targets interaction network.

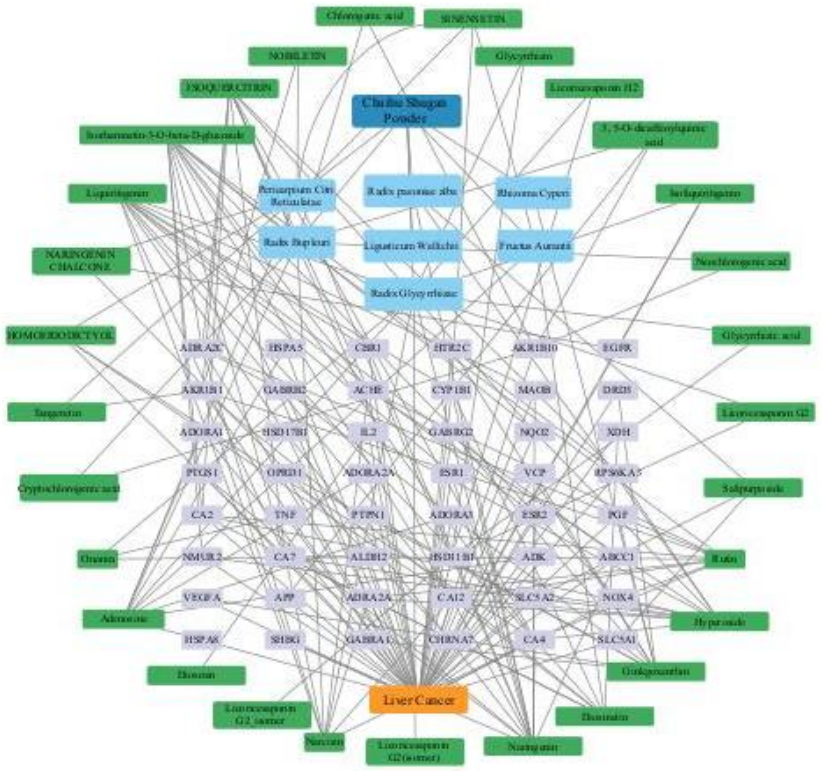


Figure 2. Network pharmacology prediction of HCC treatment with CSS. ‘Drug-component-target’ network of CSS in the treatment of HCC. ‘Compound-target’ networks of 29 core compounds and 48 targets.

2.3 Functional enrichment analysis of candidate targets

To better explore the biological roles of these 48 intersecting targets, GO and KEGG enrichment analysis was performed through the Metascape platform. GO analysis yielded a large number of significantly enriched biological processes, cellular components, and molecular functions. Based on GO analysis, regarding BP terms, the target genes are mainly enriched in cell-cell signaling, positive regulation of MAPK cascade, response to hypoxia, negative regulation of apoptotic process, cellular response to toxic substances, response to hormone, response to unfolded protein, which are all closely related to hepatocarcinogenesis and tumor development (Figure 3A).

Among CC terms, candidate targets are mainly enriched in neuron projection mem-brane, signaling receptor complex, presynaptic membrane, basolateral plasma membrane, focal adhesion, and vesicle lumen, indicating that the many targets are membrane associated proteins responsible for signal transduction (Figure 3B).

Concerning MF terms, a substantial number of molecular functions were significantly enriched, including oxidoreductase activity, carbonate dehydratase activity, neurotransmitter receptor activity, hormone binding, steroid binding, protein homodimerization activity, kinase binding and ubiquitin protein ligase binding (Figure 3C). These results suggest that CSS may regulate multiple biological processes which mediated by enzymes and receptor signals.

KEGG pathway analysis of intersecting targets further indicates that these genes were significantly enriched in multiple cancer related signaling pathways, including Chemical carcinogenesis-receptor activation, Chemical carcinogenesis - reactive oxygen species, Nitrogen metabolism, Serotonergic synapse, Neuroactive ligand-receptor inter-action, Insulin resistance, Steroid hormone biosynthesis, Folate biosynthesis and Path-ways of neurodegeneration - multiple diseases (Figure 3D). Chemical carcinogenesis, re-active oxygen species metabolism and Nitrogen metabolism are known to have strong correlations with HCC initiation and progress. Therefore, it can be inferred that CSS plays an anti-HCC effect by regulation of oxidation stress, metabolism of carcinogens, as well as various receptor mediated pathways.

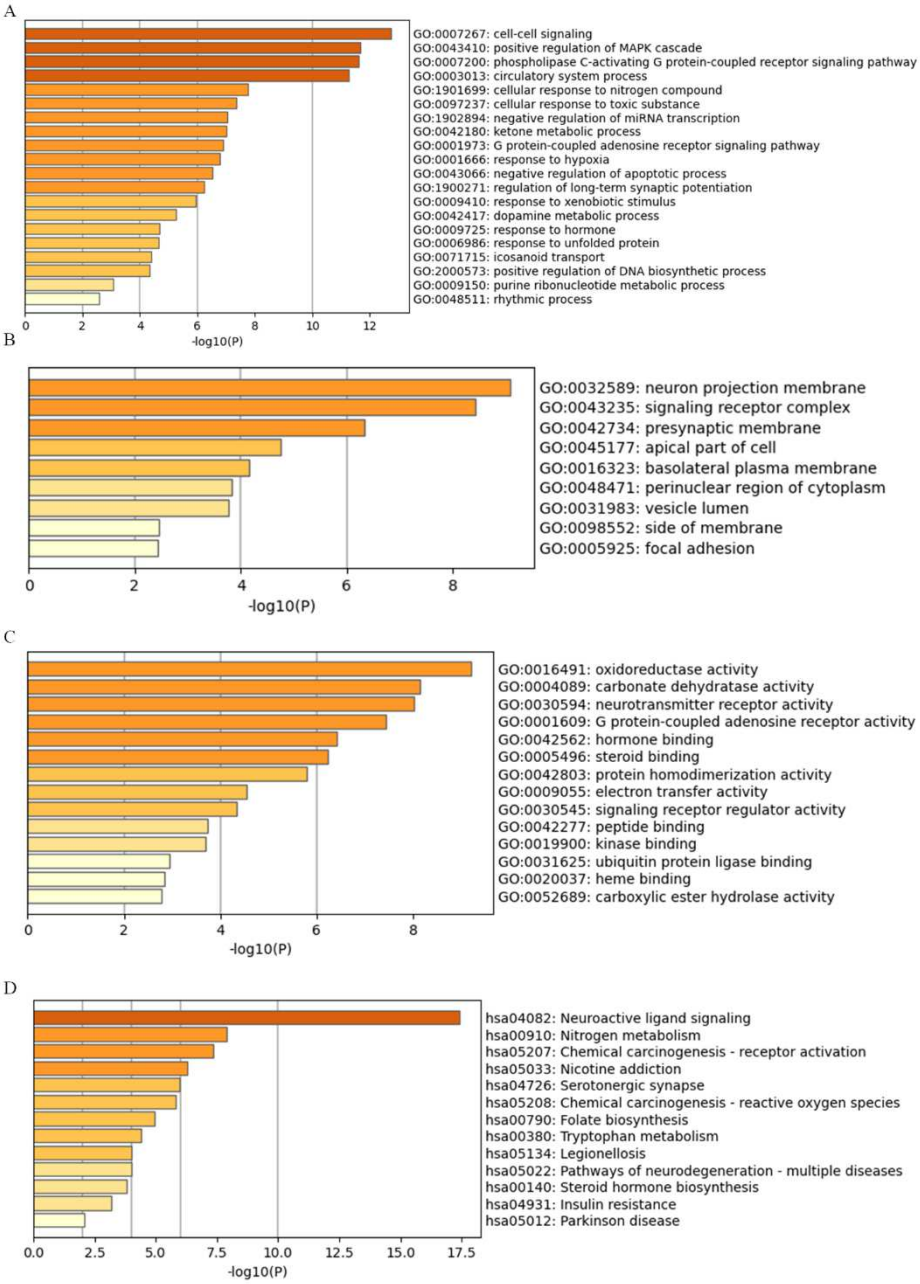


Figure 3. Functional enrichment analysis for overlapping targets. (A) Enrichment analysis for Gene Ontology biological processes (GO-BP). (B) Enrichment analysis for Gene Ontology cellular components (GO-CC). (C) Enrichment analysis for Gene Ontology molecular functions (GO-MF).

(D) Enrichment analysis for KEGG pathways. KEGG pathway information is reproduced with permission from Kanehisa Laboratories.

2.4 Identification of hub genes in the protein–protein interaction network

After analyzing the 48 intersecting targets by means of protein-protein interaction (PPI) analysis, those with potential regulatory roles in the anti-HCC activities of CSS could be screened for potential drug candidates. A network was formed among the high connectivity proteins of the intersecting targets (Figure 4A). As estimated using degrees, EGFR had the largest connectivity (degree = 12) followed by TNF (degree = 11), ESR1 (degree = 11), PTPN1 (degree = 7) as well as ADORA2A, AKR1B1, ESR2 and IL2 (degree = 5) (Figure 4B). In addition, some of the proteins with relatively high connectivity in the network including EGFR, ERS1, VEGFA, HSPA8, CA4, CA12, ALDH2, ABCC1, and CYP1B1 had been validated to be associated with HCC previously (Al-Awadhi et al., 2025; Carrera et al., 2020; Lee et al., 2023; Ning et al., 2022; Qi et al., 2023; Wang et al., 2024; Xiang et al., 2018; Xu et al., 2026). Taking account of the network topological structure and related research, EGFR, CYP1B1, VEGFA, ESR1, HSPA8, ALDH2, ABCC1, CA4, and CA12 were chosen for further molecular docking studies.

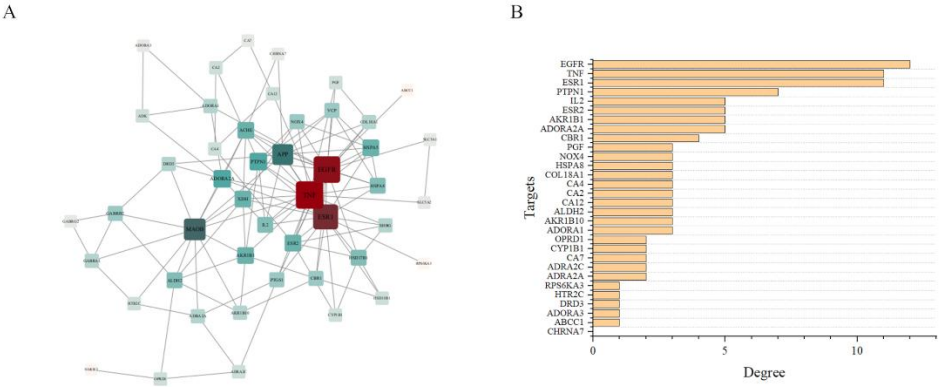


Figure 4. PPI network and the topological analysis of 48 targets (A) Construction of the PPI network with the overlapping targets of 48 selected proteins (B) The degree dis-tribution analysis of the PPI network nodes.

2.5 TCGA validation of candidate therapeutic targets

To verify the clinical significance of the selected targets, the expression profiles of the identified targets were analyzed with GEPIA2 Liver Hepatocellular Carcinoma (LIHC) dataset. Out of the nine candidate targets identified, HSPA8 and CYP1B1 showed a significant increase of expression in HCC tissues comparing to normal liver tissues. Mean-while, ALDH2, ESR1 and EGFR showed significantly lower expression in tumor samples than normal tissues. As to CA4 and CA12, no significant difference was found between tumor and normal tissues. However, there was no consistent pattern for the rest targets. Combined with the results from PPI analysis, we considered that these differential genes were involved in different stages of the process of HCC (Figure S1). In light of this finding, we nominated nine selected proteins to perform the further molecular docking and MD simulations.

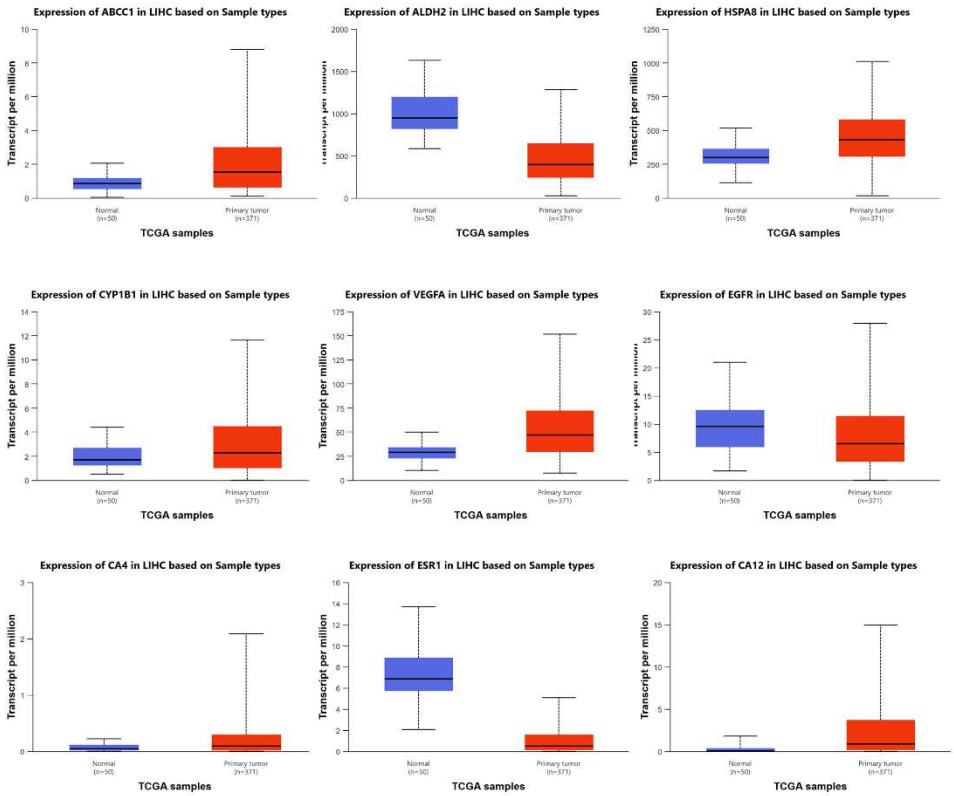


Figure S1. Expression and prognostic analysis of core targets in liver cancer.

2.6 Molecular docking identifies *Isorhoifolin* and 3,5,6,7,8,3',4'-heptamethylflavone as a potential multitarget compound

Using results of KEGG enrichment analysis, and reference of studies regarding HCC, nine proteins that closely related to progression of HCC were chose to be molecular docking receptors, namely, EGFR, CYP1B1, VEGFA, ESR1, HSPA8, ALDH2, ABCC1, CA4 and CA12. A total of 1143 protein-ligand docking pairs was created by performing docking calculation for all 121 chemical components extracted from CSS against nine identified target proteins. Among them, most compounds obtained binding affinities below -6.0 kcal/mol, suggesting good interactions with selected targets. Certain flavonoids, flavonoid glycosides, triterpenoid saponins and phenolic components presented much higher binding affinities than other polar small molecules like organic acids and amino acids (Figure 5).

Isorhoifolin and 3,5,6,7,8,3',4'-heptamethylflavone were identified as compounds with broadest spectrum, and also gave strongest binding affinity to multi target proteins. It was particularly noticed that both compounds strongly bind to EGFR and CYP1B1, two likely important pharmacological targets of CSS in HCC. *Isorhoifolin* and 3,5,6,7,8,3',4'-heptamethylflavone were chosen for further MD simulation due to their consistent well-performance on binding to different targets, and clinical approved drug Erlotinib for EGFR, CYP1B1 inhibitor 2-Phenylquinazoline-4-amine were employed as reference drugs for pharmacological comparisons.

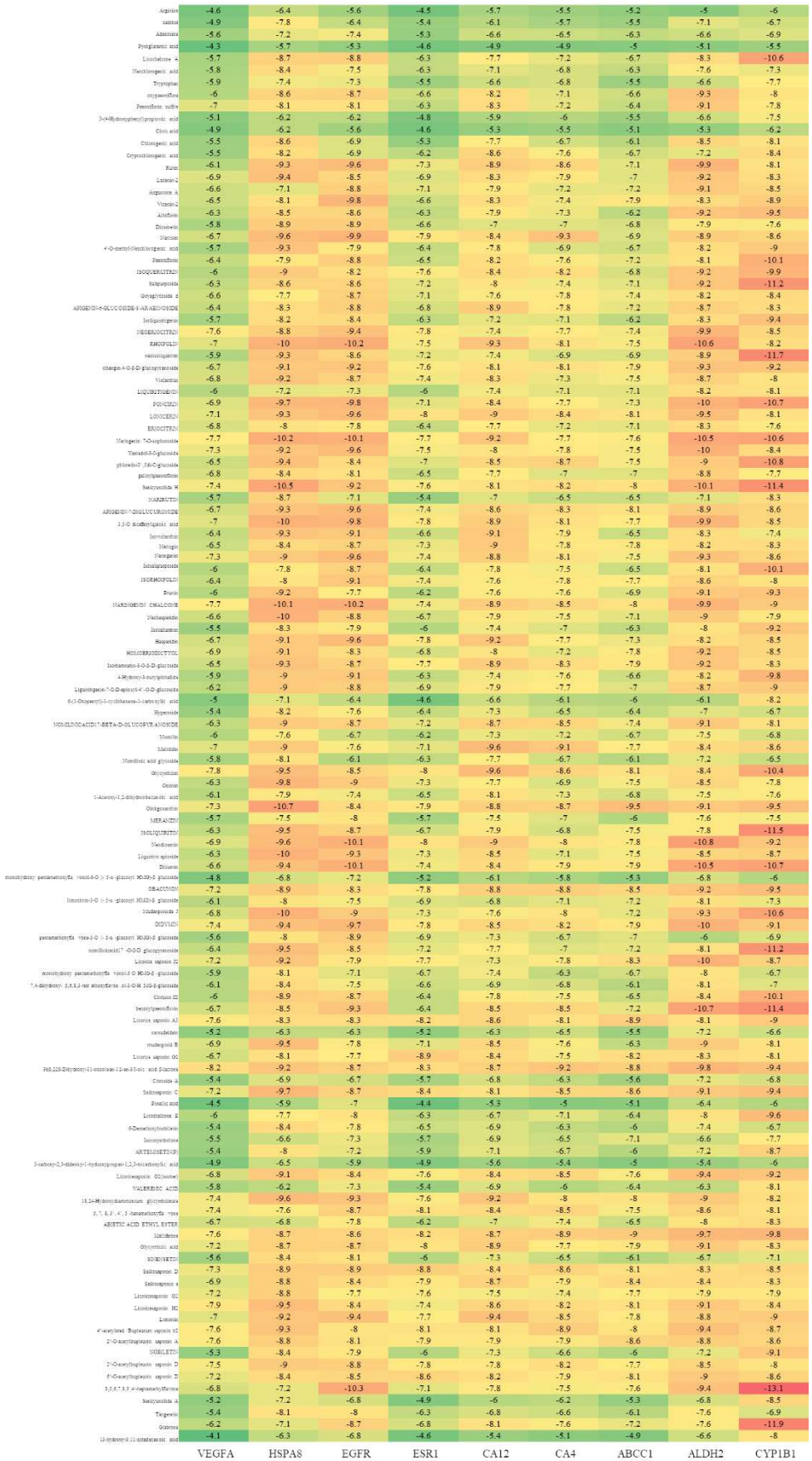


Figure 5. Heatmap of molecular docking affinities between 121 compounds and 9 core targets.

2.7 Molecular Dynamics Simulations Support Predicted Binding of *Isorhoifolin* to EGFR and CYP1B1

To further investigate the stability of ligand-protein interactions apart from static docking, 500 ns MD simulations for apo EGFR, the EGFR-*Isorhoifolin* complex, the EGFR-3,5,6,7,8,3',4'-heptamethylflavone complex, and the EGFR-Erlotinib complex was conducted. Our RMSD calculation indicated that apo EGFR had structural fluctuation of large range at early stages of the simulation and was in stable equilibrium until later stage. The EGFR-*Isorhoifolin* complex and the EGFR-Erlotinib complex was quickly con-verged and remained relatively steady state during the simulation. However, the EGFR-3,5,6,7,8,3',4'-heptamethylflavone complex maintained stable fluctuation during the entire simulation. It did not reach to steady state and implied a decreased stability than the other ligand-bound complexes (Figure S2A). Furthermore, the results of RMSF calculation also showed that several parts of EGFR became less flexibility upon binding of ligand compared with the apo state. *Isorhoifolin* demonstrated a similar fluctuation profile with Erlotinib among the three ligand complexes, which shows that *Isorhoifolin* has a similar binding effect in regulating the fluctuation characteristics of EGFR (Figure S2B). For all ligand-bound EGFR, the value of Rg was relatively stable during the entire MD simulation time, which implied that EGFR is conserved in its compactness. The Rg for the EGFR-*Isorhoifolin* complex showed less fluctuating trend compared to apo EGFR, which suggested more compacted state of EGFR upon binding *Isorhoifolin* (Figure S2C).

Meanwhile, we examined the potential interaction between *Isorhoifolin* and CYP1B1 by performing 500 ns MD simulations of CYP1B1 protein, CYP1B1-*Isorhoifolin* complex, CYP1B1-3,5,6,7,8,3',4'-heptamethylflavone complex, and CYP1B1-N-aryl-2,4-bithiazole-2-amine complex. It is shown in RMSD analysis (Figure S2D) that all ligand-bound systems tend to reach stable after equilibrium phase. It could be noticed that the conformational variation of the CYP1B1-*Isorhoifolin* complex is the minimum among all systems and reaches equilibrium earlier than the positive control complex. Analysis on the RMSF values (Figure S2E) also showed that the flexibility of most loop regions in the CYP1B1-*Isorhoifolin* complex decreased upon *Isorhoifolin* binding, compared to apo CYP1B1. This pattern of local fluctuation was similar between CYP1B1-*Isorhoifolin* complex and positive control. Rg value was also evaluated throughout the whole MD simulation (Figure S2F), indicating that none of the ligands changed the compact structure of CYP1B1 and the CYP1B1-*Isorhoifolin* complex exhibited the most stable Rg value.

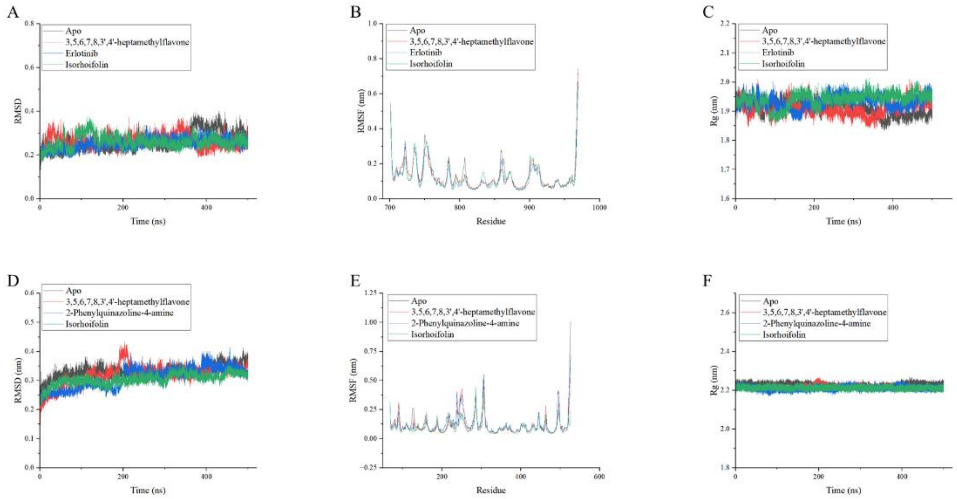


Figure S2. Trajectories analysis of protein–ligand complexes. RMSD trajectories of backbone atoms during MD simulations (A, D); RMSF profiles of amino acid residues (B, E) and Rg analysis reflecting structural compactness (C, F).

In the EGFR-*Isorhoifolin* complex, the system settled into a well-characterized low energy basin with a relatively compact distribution of conformations, suggesting good conformational stability during the simulation. Conversely, the EGFR-3,5,6,7,8,3',4'-heptamethylflavone complex exhibited a wider free energy distribution than that for the *Isorhoifolin* complex, correlating with an unstable RMSD trajectory. Furthermore, Although Erlotinib also visited a low energy region, the free energy basin for Erlotinib was less tight compared to that for *Isorhoifolin*. Similar FEL analysis was also performed for CYP1B1-inhibitor interactions; the result clearly indicates that the CYP1B1-*Isorhoifolin* complex formed the lowest and most tightly concentrated free energy basin, which suggested the highest stability of conformational state in the case of the complex, whereas relatively loose distributions were obtained in the cases of both the positive control and 3,5,6,7,8,3',4'-heptamethylflavone (Figure S3).

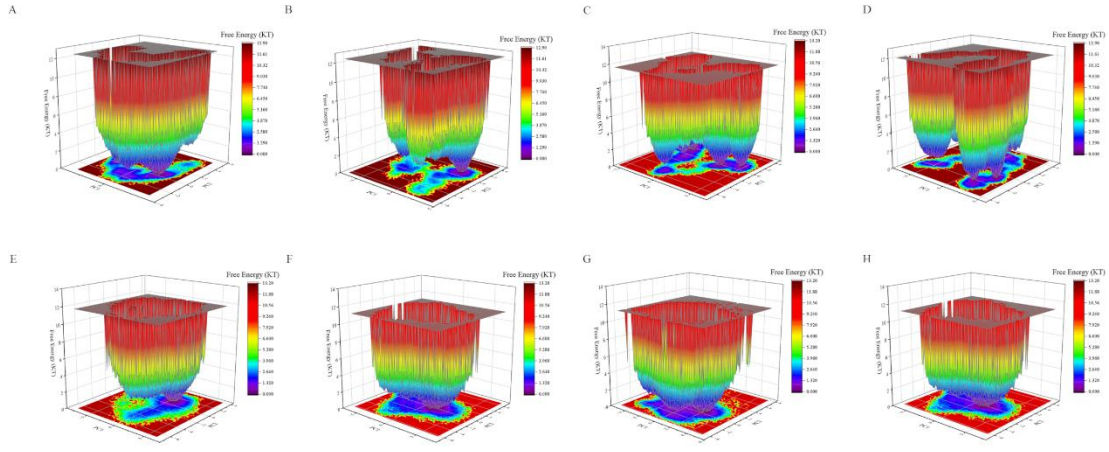


Figure S3. FEL analysis based on principal component projections. (A–D) FEL plots of CYP1B1 complexes with *Isorhoifolin*, 3,5,6,7,8,3',4'-heptamethylflavone, 2-Phenylquinazoline-4-amine, Apo form, respectively. (E-H) FEL plots of EGFR complexes with *Isorhoifolin*, 3,5,6,7,8,3',4'-heptamethylflavone, Erlotinib, Apo form, respectively. The color scale represents relative free energy levels, where blue regions indicate low-energy conformational states corresponding to higher

structural stability, and red regions represent higher-energy conformations.

In the EGFR-*Isorhoifolin* complex, the system settled into a well-characterized low energy basin with a relatively compact distribution of conformations, suggesting good conformational stability during the simulation. Conversely, the EGFR-3,5,6,7,8,3',4'-heptamethylflavone complex exhibited a wider free energy distribution than that for the *Isorhoifolin* complex, correlating with an unstable RMSD trajectory. Furthermore, Although Erlotinib also visited a low energy region, the free energy basin for Erlotinib was less tight compared to that for *Isorhoifolin*. Similar FEL analysis was also performed for CYP1B1-inhibitor interactions; the result clearly indicates that the CYP1B1-*Isorhoifolin* complex formed the lowest and most tightly concentrated free energy basin, which suggested the highest stability of conformational state in the case of the complex, whereas relatively loose distributions were obtained in the cases of both the positive control and 3,5,6,7,8,3',4'-heptamethylflavone (Figure 6).

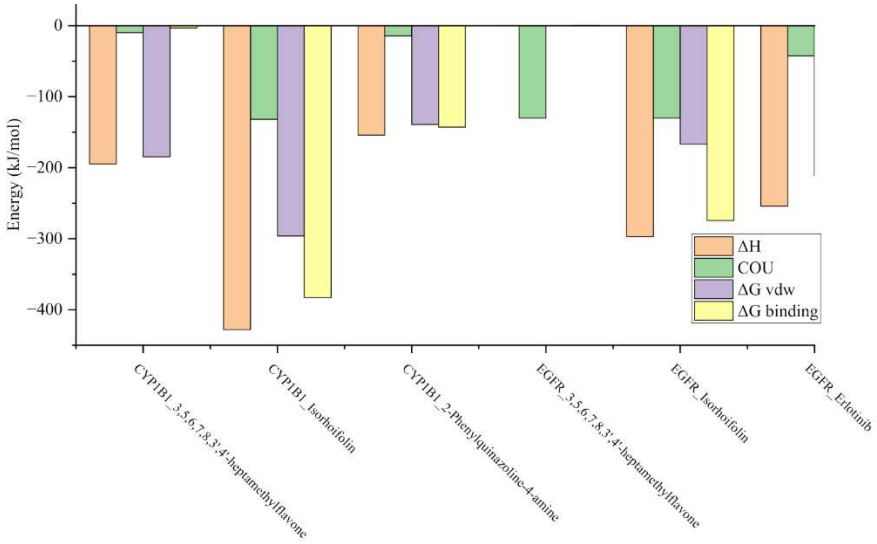


Figure 6. MM/PBSA Binding Free Energy Components of the Selected Ligand–Protein Complexes.

Together, these data strongly support that *Isorhoifolin* could bind in a more stable complex with EGFR than what can be suggested by the dock score and the second com-pound and the positive control, *Isorhoifolin* exhibited a stronger predicted binding affinity and more stable interaction pattern toward EGFR during MD simulations. MD simulations suggested that *Isorhoifolin* may interact stably with both EGFR and CYP1B1, sup-porting the hypothesis that it could act as a multitarget bioactive component.

To further investigate the mechanism of the ligand-protein interactions, some typical conformations derived from the lowest-energy basins were further investigated. *Isorhoifolin* docked into the active pocket of CYP1B1 forming a plethora of hydrogen and hydrophobic interactions with the nearby residues (Figure 7A) and had an overall inter-action pattern of the same strength as or stronger than that the positive control (Figure 7B). Similarly, *Isorhoifolin* exhibited similar trends of interaction in the case of EGFR complexes, stably interacting with several residues located in the ATP-binding area throughout the simulation (Figure 7C-D). On the whole, MD simulations showed stable complexes of *Isorhoifolin* with both EGFR and CYP1B1, providing compelling evidence for their function as potential multi-target active component of CSS in the treatment of HCC.

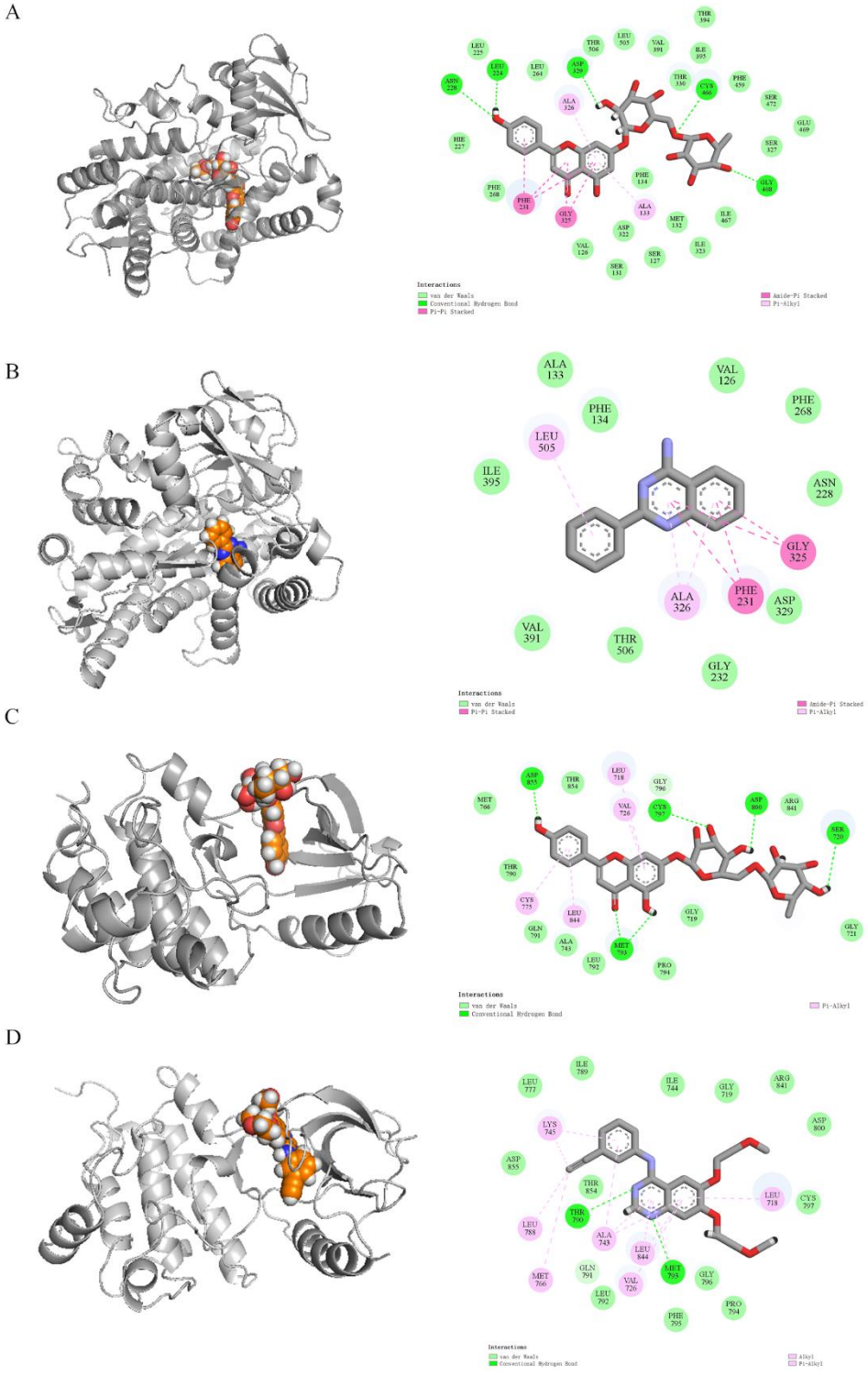


Figure 7. Structural analysis of lowest free energy conformations of *Isorhoifolin*-EGFR/CYP1B1 complexes from MD simulation. (A) *Isorhoifolin*-CYP1B1; (B) 2-Phenylquinazoline-4-amine-CYP1B1; (C) *Isorhoifolin*-EGFR; (D) Erlotinib-EGFR. (For each ligand, the left shows 3D interaction profile, and the right shows 2D interaction profile).

2.8 *Isorhoifolin* inhibits the viability and proliferation of hepatocellular carcinoma cells

Potential targeted interactions were identified by network pharmacology and MD simulation. Based on these analysis results, to verify these predictions through experiments, we further analyzed the efficacy of commercially purchased *Isorhoifolin* in two human hepatocellular carcinoma cell lines, namely HepG2 and Huh7. Viability cell assessed using the MTT assay after 48 hours of incubation with various doses of *Isorhoifolin* ranging from 1.5625 μM to 200 μM. The results showed that *Isorhoifolin* decreased the viability of both HepG2 and Huh7 cell lines in a dose-dependent manner (Figure 8A and B).

Analysis by non-linear regression estimated the half maximal inhibitory concentrations (IC50 values) to be 20.48 μM (95% confidence interval, CI: 18.86-22.30 μM) for HepG2 cells and 26.93 μM (95% CI: 24.37-29.88 μM) for Huh7 cells, suggesting that HepG2 cells were slightly more sensitive to *Isorhoifolin* treatment. We then carried out subsequent proliferation analysis with concentrations around 0.5IC50, IC50, and 2IC50 values of these cell lines (e.g., 10 μM, 20 μM and 40 μM of *Isorhoifolin* for HepG2 cells; 13 μM, 26 μM and 52 μM of *Isorhoifolin* for Huh7 cells). As seen from Figure 8C and D, there was an inhibitory effect on cell proliferation over a four-day time period with the progress of time. For HepG2 cells, the un-treated group continued to grow with exponential curve over 4 days while the groups treated with 20 μM and 40 μM could remarkably block the proliferation for a whole four-day observation, and at the highest dosage, growth of HepG2 cell had almost been inhibited when reaching the fourth day. Similar results were observed in Huh7 cells, and although inhibition of proliferation was weaker than HepG2 cells, the effect of *Isorhoifolin* on Huh7 cells was also significant and dose-dependent.

It reached a plateau of highest inhibition at highest dosage (52 μM) throughout observation. The results show that *Isorhoifolin* possessed both cell viability inhibition and proliferative capacity restriction activity to hepatocellular carcinoma cells, which coincided with predicted targeted interactions using network pharmacology and MD simulation.

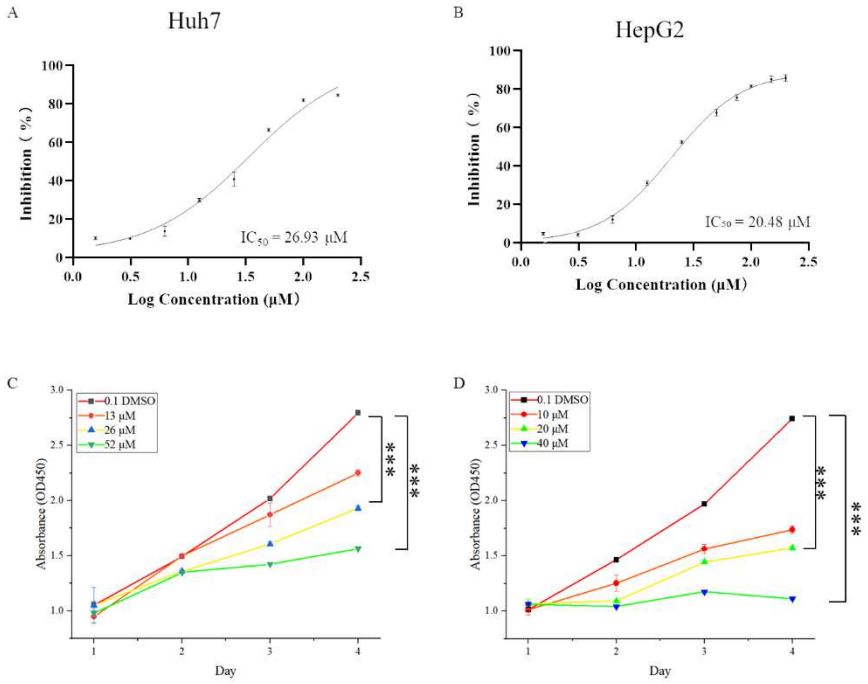


Figure 8. Dose–response analysis of *Isorhoifolin* in Huh7 and HepG2 cells. (A) Huh7 cells, (B)

HepG2 cells, and (C) Huh7 cell proliferation curve following 4 days treatment, cell viability was assessed using the MTT assay. (D) HepG2 cell proliferation curve following 4 days treatment, cell viability was assessed using the MTT assay. IC_{50} values were determined by nonlinear regression fitting (n=3). * $P < 0.05$, ** $P < 0.01$, ***$P < 0.001$ indicating significant differences in comparison to the control treatment (0.1% DMSO) group.

2.9 *Isorhoifolin* induces apoptosis in hepatocellular carcinoma cells

The impact of *Isorhoifolin* on hepatocellular carcinoma growth might involve the in-duction of apoptosis; Annexin V-FITC/PI staining and analysis by flow cytometry were carried out in HepG2 and Huh7 cells. The induction of apoptosis was determined by the quantification of the total apoptotic population (Q2 + Q3).

In Huh7 cells, low level of spontaneous apoptosis occurred in the DMSO-treated control group (5.74%), and treatment with 13 μM *Isorhoifolin* increased the rate to 16.66%, and treatment with 26 μM *Isorhoifolin* greatly induced the apoptosis to about 42.9% (Figure 9B). All data suggest that *Isorhoifolin* induces not only the proliferation inhibition of hepatocellular carcinoma cells, but also induces apoptosis dose dependently, thus, it may induce the death of hepatocellular carcinoma cells through apoptosis pathway.

In the case of HepG2 cells, spontaneous apoptosis was at a similar level to that of control group (6.16%), while 10 μM *Isorhoifolin* treatment resulted in about 17.32% apoptosis, and 20 μM *Isorhoifolin* enhanced the rate of apoptosis up to about 43.7%, revealing a significant concentration-dependent effect (Figure 9B).

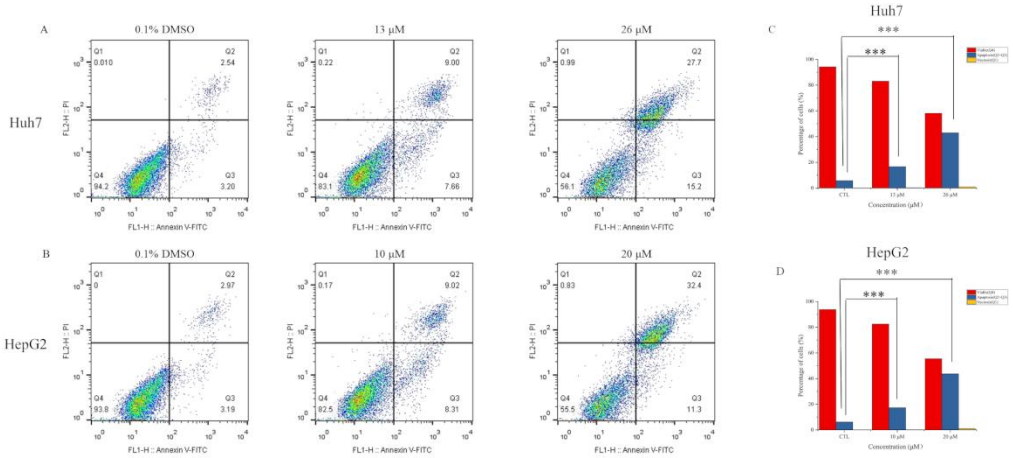


Figure 9. Effects of *Isorhoifolin* on apoptosis rate of Huh7 and HepG2 cells *In vitro*. (A, B) Apoptosis analysis by Annexin-V/PI staining. (C, D) * $P < 0.05$, ** $P < 0.01$, ** *$P < 0.001$ indicating significant differences in comparison to the control treatment (0.1% DMSO) group.

3. Discussion

HCC continues to be one of the leading causes of cancer-associated death globally, regardless of improvements made to the standard treatment for cancer like surgical re-moval, targeted therapy, or immunotherapy. Unfortunately, due to recurrent recurrence, metastatic disease, or resistance of the tumor to therapy, it's imperative to identify new strategies targeting numerous cancers promoting

pathways. TCM is composed of nu-merous molecules with multipotent effects in targeting multiple molecular pathways. Thus, it's not a surprise to consider it as a complementary treatment for cancer. As among the most frequent of classic prescriptions, it's known to regulating the liver function and relieve liver qi stagnation, however its main active components and molecular mechanisms responsible for treating HCC is still unknown. The present work applied network pharmacology and bioinformatics analysis along with other computer analysis and experimental verification for evaluating the anti-HCC ability of TCM with an overall strategy that includes identification of the overlapping targets through integration prediction targets and disease genes, functionality enrichment analysis, con-structing protein interaction network, validating with GEPIA2, Molecular Docking, long-timescale MD simulations, and experimental tests. Overall, this research concludes that *Isorhoifolin* may be a part of significant bioactive ingredients that contributed to the anti-HCC activities of CSS.

3.1 EGFR and CYP1B1 represent potential therapeutic targets of CSS

Several cancer-related signaling pathways have been uncovered by network phar-macology in the action of CSS such as the pathways of chemical carcinogenesis, reactive oxygen species, nitrogen metabolism, insulin resistance, and neuroactive ligand-receptor interaction, and it has also revealed that not only metabolism disorders, but also reactive oxygen species, the expression of xenobiotic metabolizing enzyme, and the recep-tor-mediated signaling pathway contribute to tumor development, starting from a basic research study for molecular targets of the drug or herbs used to treat cancer (Li et al., 2022; Liu et al., 2025; Xing et al., 2024).

As there were numerous overlapping target genes identified by the network phar-macology, and the biological activities associated with HCC are already published by various studies, EGFR and CYP1B1 have been further selected for deeper examination since evidence for their role in HCC was already established from either computer aided analysis or research study.

EGFR has been the most frequently targeted receptor tyrosine kinase (RTK) that contributes to proliferation, invasion, blood vessel production and resistance against the treatment of many cancers including HCC (Levantini et al., 2022). This receptor tyrosine kinase activation is mediated via signaling through the PI3K/AKT and MAPK pathways (Liu et al., 2018). It seems that EGFR signaling targeting has only been slightly effective for those patients who were unselected in the current HCC setting, but evidence sup-porting the benefit in specific molecular subtypes of HCC and potentially used as a combination therapy is growing (Heumann et al., 2024).

The members of the cytochrome P450 gene family known as CYP1B1 have an estab-lished role in activating various types of xenobiotics, controlling the level of endogenous xenobiotic, as well as controlling oxidative stress (Li et al., 2017). CYP1B1 expression has been found to be greatly elevated in most of the human malignancies, such as breast, prostate, and liver cancer, thus CYP1B1 can be found elevated in HCC as well (Kim et al., 2025). As the tissue expression level of CYP1B1 is extremely low and restricted to certain sites (e.g., liver, kidney), this gene is a very attractive therapeutic target in cancer (Yuan et al., 2022). As predicted by database, there was a significantly elevated CYP1B1 expression, whereas ALDH2 and ESR1 were significantly decreased in the tumor tissues of HCC; the change of EGFR was not significant even though its expression was slightly down.

This may suggest that the change of the expression level is not the sole factor af-fecting EGFR-

targeted therapy efficacy, the activation status rather than expression level may be another factor, or it can play a role through another pathway.

3.2 Molecular dynamics identified *Isorhoifolin* as the most promising active constituent

A highlight of this study is that molecular docking was insufficient for the prediction of the best active compound. Of the 121 compounds from CSS, *Isorhoifolin* and 3,5,6,7,8,3',4'-heptamethylflavone produced similar excellent scores toward many HCC-related targets. However, during long-time scale MD simulation, obvious differences were observed.

The binding poses of 3,5,6,7,8,3',4'-heptamethylflavone within the predicted binding pocket seemed to suffer from structural drift after relaxion, with a large degree of fluctuation around the complex of EGFR and a positive MM/PBSA binding energy, meaning that this ligand loses the favorable interaction after relaxation.

This shows that there are some limitations on standard molecular docking, where just only static poses were measured ignoring of the flexibility of protein and water molecules. Contrary, interactions between *Isorhoifolin* and the complexes of EGFR and CYP1B1 remained stable during the simulation for a longer period of 500 ns with low values of RMSD, RMSF and Rg and also reasonable MM/PBSA free energy of binding which shows that the interaction with proteins was favorable and very stable compared to others with predicted MM/PBSA binding energies even more favorable than the positive control in current computation setup. In brief, using MD to characterize the stable interactions along with docking, we are more confidently to search for stable bioactive compound compared to only use of molecular docking.

3.3 Experimental validation supports the antitumor activity of *Isorhoifolin*

In order to investigate our prediction experimentally, *Isorhoifolin* was tested on 2 human hepatocellular carcinoma cell lines. We observed a dose dependent reduction in cell viability for both HepG2 cells (IC_{50} =20.48 μM) and Huh7 cells (IC_{50} =26.93 μM) by MTT assay. Similarly, time dependent analysis of cell proliferation showed a sustained suppression of tumor cell growth throughout the4-day period while apoptosis was evident by flow cytometry.

The *in vitro* findings are thus consistent with the prediction of the multi-target binding of *Isorhoifolin*. While the specific molecular mechanisms leading to growth inhibition was not investigated here, our combined *in silico* and *in vitro* results indicate an overall potential antitumor activity of *Isorhoifolin*. Notably, because we have tested for the induction of apoptosis separately from cytotoxicity, we believe the observed rise in apoptosis is one of the factors responsible for inhibition of tumor cell growth, at least partially rather than through nonspecific toxicity.

3.4 Potential advantages of *Isorhoifolin* over its aglycone Apigenin

Isorhoifolin is a naturally occurring flavone glycoside, which the aglycone form is Apigenin, and it's the best-known flavonoid in cancer researches (Singh et al., 2022). Previous studies proved that the aglycone Apigenin has strong effects in killing hepato-carcinoma cell line. Administration with about 10 μM of Apigenin caused nearly 60-70% inhibition in cell proliferation inHuh7 and

more than 95% in HepG2, suggesting that aglycone is stronger *In vitro* cytotoxic effect than the glycoside *Isorhoifolin* (Wang et al., 2021). In order to answer whether there are benefits in the aglycone in the case of therapy *in vivo*, a series of animal studies would be performed, by means of analyzing the therapeutic effectiveness and the pharmacokinetic profile of the two compounds *in vivo*, in order to make clear if and how the glycosylation affects the *in vivo* therapeutic benefits on Hepatocarcinoma.

3.5 Limitations

The limitations of the present study are: First, although various signaling pathways involving in anti-HCC activities of CSS have been proposed by network pharmacology, no downstream mechanism was proved by experiment in the present study. Western blotting, RT-qPCR, and transcriptomic studies are needed to confirm how *Isorhoifolin* affects EGFR, CYP1B1 or others cancer related signal pathways. Second, two cell lines were tested for hepatocellular carcinoma in the current research. Whether there are similar ef-fects in another HCC model or primary HCC tumor cell is needed to clarify. Third, although MD simulations provided significant evidence for *Isorhoifolin* binding stably with EGFR and CYP1B1, the results of molecular simulations cannot fully replace of the direct biochemical experiment. Follow-up studies such as target engagement assay, activity assays of enzymes, and biophysical binding experiment need to be done. Last, this study was focused on *In vitro* studies only, *in vivo* studies with animal models will be per-formed in the next stage. Despite the continuous indications of EGFR and CYP1B1 as potential target molecules for *Isorhoifolin* by the computational analysis, target binding and downstream signaling pathways' alterations were not experimentally confirmed in this study, the mechanism needs to be addressed cautiously by future work.

4. Materials and Methods

4.1 Collection of chemical constituents of CSS

The chemical constituents of CSS were gathered from previous phytochemical re-ports. Following removal of duplicated compounds, there was a total of 121 unique constituents isolated from the 7 herbal medicines that was selected for our analysis (Table S1) (Lei et al., 2022). The canonical Simplified Molecular Input Line Entry System (SMILES) structures of all collected compounds were obtained from PubChem database (https://pubchem.ncbi.nlm.nih.gov), and then these structures were utilized for subsequent target prediction (Kim et al., 2024).

4.2 Target prediction of CSS compounds

The SMILES were imported into SwissTargetPrediction (https://www.swisstargetprediction.ch/) to predict potential human protein targets (Daina et al., 2019). The species was restricted to Homo sapiens, and only targets with a prediction probability ≥0.30 were retained. After removing duplicate entries, 48 unique targets were obtained (Table S2).

4.3 Identification of liver cancer-related targets

Liver cancer-related genes were retrieved from the GeneCards database using "liver cancer" as the search keyword (Stelzer et al., 2016). Only protein-coding genes were included, resulting in 19,063 disease-associated genes. The overlapping targets between CSS-predicted targets and liver cancer-related genes were identified using an R package, and the result was visualized using ggVennDiagram package in R version 4.4.0.

4.4 Construction of the compound–target–disease network

The intersection target was imported to Cytoscape (version 3.10.2) and constructed compound-target-disease interaction network, nodes represent medicinal herbs, active compounds, targets, HCC; edges represent interactions among them (Shannon et al., 2003).

4.5 Protein-protein interaction and functional enrichment analysis

The PPI network analysis was performed using the STRING database with a confi-dence score ≥ 0.7 (Szklarczyk et al., 2023). The interaction network was loaded into Cytoscape (version 3.10.3) and visualized. The degree value was measured to obtain the most promising target gene associated with the pharmacology efficacy of CSS to HCC (Shannon et al., 2003).

To predict the biological process, Gene Ontology (GO) and Kyoto Encyclopedia of Genes and Genomes (KEGG) enrichment analyses were conducted for the intersection targets by using the online server of Metascape (https://metascape.org). Minimum over-lap = 3, p-value cutoff = 0.01, and minimum enrichment = 1.5 were set as default analysis parameters. GO enrichment analysis consisted of three terms: Biological Process (BP), Cellular Component (CC), and Molecular Function (MF). Significantly enriched pathways associated with HCC by KEGG were screened. KEGG is a knowledgebase for systematic analysis of gene functions and biological pathways (Kanehisa & Goto, 2000; Kanehisa et al., 2016).

4.6 Survival and Expression Analysis

To evaluate the clinical utility of identified targets, the expression profile analysis for the selected targets were obtained from the LIHC a web server, GEPIA2 (http://gepia2.cancer-pku.cn/), that integrates data from The Cancer Genome Atlas (TCGA) and the Genotype-Tissue Expression (GTEx) project (Tang et al., 2019). mRNA expression levels of EGFR, ESR1, HSPA8, ALDH2, CYP1B1, VEGFA, CA4, CA12 and ABCC1 in tumor tissues were compared with that in adjacent non-tumorous tissues of LIHC patients. Significant differential expressed genes were identified as preferred for molecular docking analysis.

4.7 Molecular docking

All 121 identified compounds were docked against the selected targets. Erlotinib and

2-phenylquinazolin-4-amines were employed as reference inhibitors for EGFR and CYP1B1, respectively, and were docked using the same protocol (Philip et al., 2005; Yang et al., 2024). Docking scores were used to evaluate ligand–protein binding affinity. The 3D crystal structures for the selected protein targets were downloaded from the Protein Data Bank (Berman et al., 2000). The protein structures were prepared by removing water molecules and co-crystallized ligands. Polar hydrogens were added to the structure; non-polar hydrogens were merged; and Gasteiger charges were assigned to both the protein and ligands. The docking grid box was set to cover the entire protein structure of each target. Molecular docking was performed using AutoDock Vina (version 1.1.1) (Trott & Olson, 2010) using an exhaustiveness of 100. The docking was performed only once for each ligand, generating up to 10 possible binding poses (modes = 10). The top-ranking binding pose with the lowest binding energy was chosen and later molecular dynamics simulations. Visual inspection was carried out on the docked conformations with the use of Discovery Studio (4.5). Details of the docking parameters can be seen in Table S3. The docking results were validated for each target protein using its respective known reference ligand.

4.8 Molecular dynamics simulation

MD simulation was performed in the GROMACS package (Páll et al., 2020). The protein structure was described by the AMBER ff19SB force field (Tian et al., 2020). The parameters of ligand were generated by the General Amber Force Field (GAFF) and converted to GROMACS format using ACPYPE (Sousa da Silva & Vranken, 2012; Wang et al., 2004). The protein-ligand complex was immersed in a cubic box with TIP3P explicit water molecules with a distance between protein surface and boundary of box greater than 1.0 nm. Appropriate number of counter-ions were added to neutralize the charge of the system and a 0.15 M concentration of NaCl were used for simulating the physiological ionic strength. Steric clash and unfavorable interaction were removed by steepest descent method to achieve the energy minimization for convergence. Then, the system was re-laxed for 100 ps in NVT ensemble to equilibrate the temperature by apply position restraints on the protein. Afterwards, NPT ensemble run for 1 ns was carried out to balance the pressure by apply the coupling pressure. The temperature was maintained at 310.15 K by using V-rescale thermostat with 0.1 ps coupling time. The pressure was kept at 1 bar by using Parrinello-Rahman barostat with isotropic coupling method and time constant of 2.0 ps, with a compressibility of 4.5 x 10^{-5} bar.

For the production run of MD simulation, the leap-frog integration algorithm with time step of 2 fs for 500 ns was applied under periodic boundary conditions. Periodic boundary conditions and leap-frog algorithm were used with time step of 2 fs for 500 ns (250,000,000 steps). All the bonds with hydrogen atoms were constrained using LINCS algorithm. Verlet cutoff scheme was used for neighbor searching, and neighbors were updated every 20 fs. The electrostatics and vdW calculations were treated by PME method for long-range electrostatic interactions and a cutoff of 1.0 nm was applied for short range electrostatics and vdW interactions. A switching function over 0.95–1.0 nm was applied for vdW interactions. PME was used to calculate the long-range electrostatic interactions with a Fourier grid spacing of 0.16 nm and fourth-order interpolation scheme. Dispersion correction was used for both energy and pressure. Velocities were not rei-nitialized during the production run and MD was initiated from the equilibrated NPT ensemble. Structural stability and dynamics of protein–ligand complex was investigated using GROMACS

built-in tools: Root mean square deviation (RMSD), Root mean square fluctuation (RMSF) and Radius of gyration (Rg) were computed. FEL was constructed based on projecting PC1 and PC2 onto the data of MD trajectories by using principal component analysis (PCA) method and the bottom of FEL was identified by using Crucial Interval Calculation package through the density method (Wei et al., 2025).

4.9 MM-PBSA Binding Free Energy Calculation

Binding free energies were calculated using gmx_MMPBSA workflow together with APBS in equilibrated MD trajectories (Baker et al., 2001). Snapshots were extracted from FEL to perform MM-PBSA calculation, and frame with lowest free energy was picked as center and 50 frames before and after that were used (totally 100 frames). Dielectric constants for solute and solvent were 2 and 78.54, respectively, and the commonly used ones in protein-solvent system. Ionic strength was 0.15M and temperature was 310.15K. Polar solvation energy was calculated using non-linear Poisson-Boltzmann equation (NPBE) by using solvent probe radius 1.4 Å. Non-polar solvation was obtained from SASA (solvent-accessible surface area) with solvent tension coefficient of 1 kJ/mol. Binding free energy (ΔG_bind) was obtained using the formula: ΔG_bind = ΔE_MM +ΔG_PB + ΔG_SA -ΔTS, wherein ΔE_MM is the contribution of molecular mechanics including vdw and electrostatic energies, ΔG_PB is the polar solvation energy, ΔG_SA is the non-polar solvation energy and ΔTS is the entropy contributions calculated by the interaction entropy (IE) method. Furthermore, per residue energy decomposition was also performed in order to identify the amino acids most involved in binding of the ligand.

4.10 Cell culture and Cell Viability Assay

Huh7 (SCSP-526) and HepG2 (TCHu72) human hepatocellular carcinoma cell lines were obtained from the Cell Bank of the Chinese Academy of Sciences (Shanghai, China). The cell lines HepG2 and Huh7 were cultured in Dulbecco's Modified Eagle Medium (DMEM, Gibco, USA) containing 10% fetal bovine serum (FBS) and 1% penicillin-streptomycin in a humidified incubator with 5% CO_2 at 37°C.

Cell viability was assessed by the MTT assay. The cells were seeded in 96-well plates, and then treated with the *Isorhoifolin* tested at a concentration range of 1.56, 3.13, 6.25, 12.50, 25.00, 50.00, 75.00,100.00, 150.0, 200.0 μM. After 24 h incubation at 37°C, MTT solution was added and cells were further incubated for 4 h to form purple formazan crystals. Supernatant was carefully removed and the crystals were dissolved in DMSO, followed by measurement of absorbance at 570 nm using a microplate reader (BioTek Synergy H1, Agilent Technologies, USA). IC_{50} was determined by non-linear regression using GraphPad Prism software (version 9.6, GraphPad Software, USA).

4.11 Apoptosis Analysis by Flow Cytometry

The Annexin V/ PI double staining flow cytometry method was used to analyze apoptosis. Cells were cultured and treated with the compounds in con-centrations of 20, 40 μM for HepG2 cells ($1x10^4$/well) and 26, 52 μM for Huh7 cells ($1x10^4$/well) at 37°C for 24 h, respectively. After

treatments, the cells were washed twice with cold Phosphate-Buffered Saline (PBS) and then collected by centrifugation. Cell pellets were suspended in 100 μL of binding buffer and incubated with 5 μL Annexin V-APC and 5 μL PI in a dark room at 25 ℃ for 15 min. Finally, 400 μL binding buffer was added, and the mixture was immediately collected and washed twice with cold PBS for flow cytometric analysis. Flow cytometry was carried out using a LSR Fortessa flow cy-tometer (BD Biosciences, USA), and 10,000 events per sample were acquired. FlowJo software (version 10.8.1) was employed for data analysis, and quadrant gating was set to define viable cells, early apoptotic cells, late apoptotic cells, and necrotic cells. The experiments were independently performed three times, and results are expressed as mean SD. Statistical significance was assessed by one-way ANOVA, with $P < 0.05$ deemed significant.

5. Conclusions

In summary, this study used network pharmacology combined with bioinformatics, molecular docking, MD simulation and experimental verification workflows to reveal in an organized manner the molecular pharmacological mechanisms underlying CSS in treating hepatocellular carcinoma. 48 candidate therapeutic targets were obtained, and enrichment analyses revealed various biological processes and signal transduction pathways associated with cancer. Both molecular docking and long-timescale MD simulations strongly indicated that *Isorhoifolin* was the best candidate drug for the active component based on stable binding to the targets EGFR and CYP1B1 and optimal free-energy values. *Isorhoifolin* obviously attenuated hepatocellular carcinoma cell viability and growth while promoting apoptosis of both HepG2 and Huh7 cells.

Based on the comprehensive results of this study, *Isorhoifolin* demonstrated anti-HCC activity *In vitro* and showed predicted interactions with EGFR and CYP1B1. Further studies are required to experimentally validate these molecular targets and elucidate the mechanisms., thus serving a theoretical reference and experimental evidence basis for mechanism researches and clinical applications of this compound.

Author Contributions: Conceptualization, X.J. And Y.Z; methodology, X.J.; software, X.J.; validation, F.L., C.C. and H.Y.; formal analysis, L.S.; investigation, J.X.; resources, N.L.; data curation, X.J.; writing—original draft preparation, X.J.; writing—review and editing, F.L., C.C., and Y.Z.; visualization, C.C.; supervision, Z.Y.; project administration, Y.Z.; funding acquisition, Y.Z. All authors have read and agreed to the published version of the manuscript.

Funding: This research received no external funding

Conflicts of Interest: The authors declare no conflicts of interest.

Abbreviations

CSS	*Chaihu Shugan San*
HCC	Hepatocellular carcinoma
MD	Molecular dynamics
FEL	Free energy landscape
TCM	Traditional Chinese medicine

PPI	Protein–protein interaction
MM/PBSA	Molecular Mechanics/Poisson–Boltzmann Surface Area
SMILES	Simplified Molecular Input Line Entry System
GO	Gene Ontology
MF	Molecular Function
BP	Biological Process
CC	Cellular Component
KEGG	Kyoto Encyclopedia of Genes and Genomes
LIHC	Liver Hepatocellular Carcinoma
TCGA	The Cancer Genome Atlas
GTEx	Genotype-Tissue Expression
GAFF	General Amber Force Field
RMSD	Root mean square deviation
RMSF	Root mean square fluctuation
Rg	Radius of gyration
PCA	Principal component analysis
NPBE	Non-linear Poisson-Boltzmann equation
SASA	Solvent-accessible surface area
IE	Interaction entropy
DMEM	Dulbecco's Modified Eagle Medium
FBS	fetal bovine serum
PI	Propidium iodide
PBS	Phosphate-Buffered Saline

References

1. Al-Awadhi, S. S. A., Patil, P., Shetty, P., Shetty, P. K., Shetty, R. A., & Shetty, V. V. (2025). Potential role of epidermal growth factor receptors (EGFR) signaling in the pathogenesis and management of hepatocellular carcinoma. Bioimpacts, 15. https://doi.org/0.34172/bi.30905

2. Baker, N. A., Sept, D., Joseph, S., Holst, M. J., & McCammon, J. A. (2001). Electrostatics of nanosystems: Application to micro-tubules and the ribosome. Proceedings of the National Academy of Sciences of the United States of America, 98(18), 10037-10041. https://doi.org/10.1073/pnas.181342398

3. Berman, H. M., Westbrook, J., Feng, Z., Gilliland, G., Bhat, T. N., Weissig, H., Shindyalov, I. N., & Bourne, P. E. (2000). The Protein Data Bank. Nucleic Acids Research, 28(1), 235-242. https://doi.org/10.1093/nar/28.1.235

4. Carrera, A. N., Grant, M. K. O., & Zordoky, B. N. (2020). CYP1B1 as a therapeutic target in cardio-oncology. Clinical Science, 134(21), 2897-2927. https://doi.org/10.1042/Cs20200310

5. Chidambaranathan-Reghupaty, S., Fisher, P. B., & Sarkar, D. (2021). Hepatocellular carcinoma (HCC): Epidemiology, etiology and molecular classification. Mechanisms and Therapy of Liver Cancer, 149, 1-61. https://doi.org/10.1016/bs.acr.2020.10.001

6. Daina, A., Michielin, O., & Zoete, V. (2019). SwissTargetPrediction: updated data and new features for efficient prediction of protein targets of small molecules. Nucleic Acids Research, 47(W1), W357-W364. https://doi.org/10.1093/nar/gkz382

7. Heumann, P., Albert, A., Guelow, K., Tümen, D., Mueller, M., & Kandulski, A. (2024). Insights in Molecular Therapies for Hepatocellular Carcinoma. Cancers, 16(10). http://doi.org/10.3390/cancers16101831

8. Kim, J. W., Tung, H. C., Yang, B., Pant, R., Guan, X. C., Feng, Y., & Xie, W. (2025). Heme-thiolate monooxygenase cytochrome P450 1B1, an old dog with many new tricks. Pharmacological Reviews, 77(3). https://doi.org/10.1016/j.pharmr.2025.100045

9. Kim, S., Chen, J., Cheng, T. J., Gindulyte, A., He, J., He, S. Q., Li, Q. L., Shoemaker, B. A., Thiessen, P. A., Yu, B., Zaslavsky, L., Zhang, J., & Bolton, E. E. (2024). PubChem 2025 update. Nucleic Acids Research, 53(D1), D1516-D1525. https://doi.org/10.1093/nar/gkae1059

10. Ladd, A. D., Duarte, S., Sahin, I., & Zarrinpar, A. (2024). Mechanisms of drug resistance in HCC. Hepatology, 79(4), 926-940. https://doi.org/10.1097/Hep.0000000000000237

11. Lee, S. J., Toft, N. J., Axelsen, T. V., Espejo, M. S., Pedersen, T. M., Mele, M., Pedersen, H. L., Balling, E., Johansen, T., Burton, M., Thomassen, M., Vahl, P., Christiansen, P., & Boedtkjer, E. (2023). Carbonic anhydrases reduce the acidity of the tumor micro-environment, promote immune infiltration, decelerate tumor growth, and improve survival in ErbB2/HER2-enriched breast cancer. Breast Cancer Research, 25(1). https://doi.org/10.1186/s13058-023-01644-1

12. Lei, S. S., Zhao, S., Huang, X. Y., Feng, Y. C., Li, Z. S., Chen, L., Huang, P. Y., Guan, H. S., Zhang, H. B., Wu, Q. H., & Chen, B. J. (2022). Chaihu Shugan powder alleviates liver inflammation and hepatic steatosis in NAFLD mice: A network pharmacology study and experimental validation. Frontiers in Pharmacology, 13. https://doi.org/10.3389/fphar.2022.967623

13. Levantini, E., Maroni, G., Del Re, M., & Tenen, D. G. (2022). EGFR signaling pathway as therapeutic target in human cancers. Seminars in Cancer Biology, 85, 253-275. https://doi.org/10.1016/j.semcancer.2022.04.002

14. Li, F., Zhu, W. F., & Gonzalez, F. J. (2017). Potential role of CYP1B1 in the development and treatment of metabolic diseases. Pharmacology & Therapeutics, 178, 18-30. https://doi.org/10.1016/j.pharmthera.2017.03.007

15. Li, P., Ding, Z., Feng, Y. Q., Ren, X. Y., Wei, Y. Y., Xia, C. F., Yang, Y. T., Yang, Q. B., Wang, Z., Zhang, X. H., van der Geest, L. G., Yu, H., Giovannucci, E., Smith, D. P., David, M., Jemal, A., Yu, X. Q., Zeng, H. M., & Cao, G. W. (2026). Global, regional, and national burden of hepatocellular carcinoma and contribution of nine modifiable risk factors across 185 countries/territories in 2022. Science Bulletin, 71(4), 838-849. https://doi.org/10.1016/j.scib.2025.12.022

16. Li, S. Q., Chen, X., Shi, H., Yi, M., Xiong, B., & Li, T. Y. (2025). Tailoring traditional Chinese medicine in cancer therapy. Molec-ular Cancer, 24(1). https://doi.org/10.1186/s12943-024-02213-6

17. Li, W., Zhou, R. Z., Zheng, J., Sun, B., Jin, X., Hong, M., & Chen, R. N. (2022). Chaihu-Shugan-San ameliorates tumor growth in prostate cancer promoted by depression modulating sphingolipid and glycerinphospholipid metabolism. Frontiers in Phar-macology, 13. https://doi.org/10.3389/fphar.2022.1011450

18. Liu, F., Li, L. N., Zhang, Y. M., Zhang, J. Q., Tian, X. C., Zhang, D. T., Zhang, N., Yan, T. H., Shi, S. L., Wu, J. L., & Jiang, S. L. (2025). Mechanistic Exploration of Shugan Jianpi Formula for Treating Triple-Negative Breast Cancer Under Chronic Stress: A Net-work Pharmacology-Guided Experimental Study. Drug Design Development and Therapy, 19, 4585-4603. https://doi.org/10.2147/Dddt.S518123

19. Liu, Q., Yu, S. N., Zhao, W. H., Qin, S., Chu, Q., & Wu, K. M. (2018). EGFR-TKIs resistance via EGFR-independent signaling pathways. Molecular Cancer, 17. https://doi.org/10.1186/s12943-018-0793-1

20. Ning, W. R., Jiang, D., Liu, X. C., Huang, Y. F., Peng, Z. P., Jiang, Z. Z., Kang, T. B., Zhuang, S. M., Wu, Y., & Zheng, L. M. (2022). Carbonic anhydrase XII mediates the survival and prometastatic functions of macrophages in human hepatocellular carcinoma. Journal of Clinical Investigation, 132(7). https://doi.org/ https://doi.org/10.1172/JCI153110

21. Páll, S., Zhmurov, A., Bauer, P., Abraham, M., Lundborg, M., Gray, A., Hess, B., & Lindahl, E. (2020).

Heterogeneous parallel-ization and acceleration of molecular dynamics simulations in GROMACS. J Chem Phys, 153(13), 134110. https://doi.org/10.1063/5.0018516

22. Philip, P. A., Mahoney, M. R., Allmer, C., Thomas, J., Pitot, H. C., Kim, G., Donehower, R. C., Fitch, T., Picus, J., & Erlichman, C. (2005). Phase II study of erlotinib (OSI-774) in patients with advanced hepatocellular cancer. Journal of Clinical Oncology, 23(27), 6657-6663. https://doi.org/10.1200/Jco.2005.14.696

23. Qi, Y. C., Song, Y. H., Cai, M. T., Li, J. W., Yu, Z. T., Li, Y. H., Huang, J. K., Jiang, Y., Peng, C., Jiang, B., & Liu, S. L. (2023). Vascular endothelial growth factor A is a potential prognostic biomarker and correlates with immune cell infiltration in hepatocellular carcinoma. Journal of Cellular and Molecular Medicine, 27(4), 538-552. https://doi.org/10.1111/jcmm.17678

24. Shannon, P., Markiel, A., Ozier, O., Baliga, N. S., Wang, J. T., Ramage, D., Amin, N., Schwikowski, B., & Ideker, T. (2003). Cy-toscape: a software environment for integrated models of biomolecular interaction networks. Genome Res, 13(11), 2498-2504. https://doi.org/10.1101/gr.1239303

25. Singh, D., Gupta, M., Sarwat, M., & Siddique, H. R. (2022). Apigenin in cancer prevention and therapy: A systematic review and meta-analysis of animal models. Critical Reviews in Oncology Hematology, 176. https://doi.org/10.3389/fonc.2021.657665

26. Sousa da Silva, A. W., & Vranken, W. F. (2012). ACPYPE - AnteChamber PYthon Parser interfacE. BMC Res Notes, 5, 367. https://doi.org/10.1186/1756-0500-5-367

27. Stelzer, G., Rosen, N., Plaschkes, I., Zimmerman, S., Twik, M., Fishilevich, S., Stein, T. I., Nudel, R., Lieder, I., Mazor, Y., Kaplan, S., Dahary, D., Warshawsky, D., Guan-Golan, Y., Kohn, A., Rappaport, N., Safran, M., & Lancet, D. (2016). The GeneCards Suite: From Gene Data Mining to Disease Genome Sequence Analyses. Curr Protoc Bioinformatics, 54, 1 30 31-31 30 33. https://doi.org/10.1002/cpbi.5

28. Szklarczyk, D., Kirsch, R., Koutrouli, M., Nastou, K., Mehryary, F., Hachilif, R., Gable, A. L., Fang, T., Doncheva, N. T., Pyysalo, S., Bork, P., Jensen, L. J., & von Mering, C. (2023). The STRING database in 2023: protein-protein association networks and functional enrichment analyses for any sequenced genome of interest. Nucleic Acids Res, 51(D1), D638-d646. https://doi.org/10.1093/nar/gkac1000

29. Tang, Z., Kang, B., Li, C., Chen, T., & Zhang, Z. (2019). GEPIA2: an enhanced web server for large-scale expression profiling and interactive analysis. Nucleic Acids Res, 47(W1), W556-w560. https://doi.org/10.1093/nar/gkz430

30. Tian, C., Kasavajhala, K., Belfon, K. A. A., Raguette, L., Huang, H., Migues, A. N., Bickel, J., Wang, Y., Pincay, J., Wu, Q., & Simmerling, C. (2020). ff19SB: Amino-Acid-Specific Protein Backbone Parameters Trained against Quantum Mechanics Energy Surfaces in Solution. Journal of Chemical Theory and Computation, 16(1), 528-552. https://doi.org/10.1021/acs.jctc.9b00591

31. Trott, O., & Olson, A. J. (2010). AutoDock Vina: improving the speed and accuracy of docking with a new scoring function, efficient optimization, and multithreading. J Comput Chem, 31(2), 455-461. https://doi.org/10.1002/jcc.21334

32. Wang, J., Wolf, R. M., Caldwell, J. W., Kollman, P. A., & Case, D. A. (2004). Development and testing of a general amber force field. Journal of Computational Chemistry, 25(9), 1157-1174. https://doi.org/10.1002/jcc.20035

33. Wang, S. M., Yang, P. W., Feng, X. J., Zhu, Y. W., Qiu, F. J., Hu, X. D., & Zhang, S. H. (2021). Apigenin Inhibits the Growth of Hepatocellular Carcinoma Cells by Affecting the Expression of microRNA Transcriptome. Frontiers in Oncology, 11. https://doi.org/10.3389/fonc.2021.657665

34. Wang, T. T., Rao, D., Fu, C. A., Luo, Y. M., Lu, J. L., Liang, H. F., Xia, L. M., & Huang, W. J. (2024). Pan-cancer analysis of ABCC1 as a potential prognostic and immunological biomarker. Translational Oncology, 41. https://doi.org/10.1016/j.tranon.2024.101882

35. Wei, C., Heh, C. H., & Chin, S. P. (2025). Selective Stabilization of LRRK2 Kinase Conformations Reveals

Distinct Modes of Action for Type I and II Inhibitors. Cell Biochem Biophys. https://doi.org/10.1007/s12013-025-01877-1

36. Xiang, X., You, X. M., & Li, L. Q. (2018). Expression of HSP90AA1/HSPA8 in hepatocellular carcinoma patients with depression. Onco Targets Ther, 11, 3013-3023. https://doi.org/10.2147/OTT.S159432

37. Xie, Z. H., Xie, Z. Y., Trujillo, N. P., Yang, T., & Yang, C. X. (2022). Exploring mechanisms of Chaihu-Shugan-San against liver fibrosis by integrated multi-omics and network pharmacology approach. Bioscience Reports, 42(7). https://doi.org/10.1042/BSR20221030

38. Xing, J. H., Tan, R. X., Huang, F. E., & Tian, N. (2024). Integrated analyses for identification of a three-gene signature associated with Chaihu Shugan San formula for hepatocellular carcinoma treatment. Journal of Cellular and Molecular Medicine, 28(8). https://doi.org/10.1111/jcmm.18211

39. Xu, H., Li, Y. P., Zhao, R., Ma, S. W., Hu, N., Yu, S., & Lv, X. F. (2026). Integrated Bulk and Single-Cell Transcriptomic Analysis Reveals Xenobiotic Metabolism Genes Drive Progression From Liver Cirrhosis to Hepatocellular Carcinoma. Human Mutation, 2026(1). https://doi.org/10.1155/humu/6845605

40. Yang, M. X., Yang, F. Y., Huang, X. Y., Cai, J. J., Zhang, Y. X., Jia, J. H., & Qiu, D. C. (2024). Design of Novel 2-Phenylquinazolin-4-amines as Selective CYP1B1 Inhibitors for Overcoming Paclitaxel Resistance in A549 Cells. Journal of Medicinal Chemistry, 67(7), 5883-5901. https://doi.org/10.1021/acs.jmedchem.4c00164

41. Ye, L. M., Liu, Y. W., Peng, X. T., & He, M. Y. (2026). Computational renaissance in herbal medicine: A 20-year bibliometric deciphering of molecular dynamics simulations reshaping traditional Chinese medicine drug discovery. Saudi Pharmaceutical Journal, 34(2). https://doi.org/10.1007/s44446-026-00080-4

42. Yuan, B. C., Liu, G. H., Dai, Z. L., Wang, L., Lin, B. S., & Zhang, J. (2022). CYP1B1: A Novel Molecular Biomarker Predicts Mo-lecular Subtype, Tumor Microenvironment, and Immune Response in 33 Cancers. Cancers, 14(22). https://doi.org/10.3390/cancers14225641

43. Zhai, Y. Y., Liu, L., Zhang, F. Q., Chen, X. D., Wang, H. J., Zhou, J. Y., Chai, K. Y., Liu, J. Y., Lei, H. L., Lu, P. Y., Guo, M. L., Guo, J. C., & Wu, J. R. (2025). Network pharmacology: a crucial approach in traditional Chinese medicine research. Chinese Medicine, 20(1). https://doi.org/10.1186/s13020-024-01056-z

44. Zhang, X. H., Zhao, Q. L., Wang, Y., Mao, Y. Q., Sun, Y., & Bian, X. K. (2024). Effectiveness and safety of Chaihu-Shugan-San for treating depression based on clinical cases: An updated systematic review and meta-analysis. Medicine, 103(26). https://doi.org/10.1097/MD.0000000000038668

45. Kanehisa, M., & Goto, S. (2000). KEGG: Kyoto Encyclopedia of Genes and Genomes. Nucleic Acids Research, 28(1), 27-30. https://doi.org/DOI 10.1093/nar/28.1.27

46. Kanehisa, M., Sato, Y., Kawashima, M., Furumichi, M., & Tanabe, M. (2016). KEGG as a reference resource for gene and protein annotation. Nucleic Acids Research, 44(D1), D457-D462. https://doi.org/10.1093/nar/gkv1070

Supplementary Files

This is a list of supplementary files associated with this preprint. Click to download.

- TableS1.docx
- TableS2.docx
- TableS3.docx
- FigureS1.pdf
- FigureS2.pdf
- FigureS3.pdf